The heterologous expression of a plastocyanin in the diatom *Phaeodactylum tricornutum* improves cell growth under iron-deficient conditions

Carmen Castell[1], Pilar Bernal-Bayard[1], José M. Ortega[1], Mercedes Roncel[1], Manuel Hervás[1], José A. Navarro[1*]

[1]Instituto de Bioquímica Vegetal y Fotosíntesis, cicCartuja, Universidad de Sevilla and CSIC, Seville, Spain.

*Corresponding author: José A. Navarro, Instituto de Bioquímica Vegetal y Fotosíntesis, Centro de Investigaciones Científicas Isla de la Cartuja, Universidad de Sevilla and CSIC, Américo Vespucio 49, 41092-Sevilla, Spain; E-mail: jnavarro@ibvf.csic.es

This is the pre-peer-reviewed version of the following article:
The heterologous expression of a plastocyanin in the diatom Phaeodactylum tricornutum improves cell growth under iron-deficient conditions
http://dx.doi.org/10.1111/ppl.13290

ABSTRACT

We have investigated if the heterologous expression in the diatom *Phaeodactylum tricornutum* of a functional green alga plastocyanin, as an alternative to cytochrome c_6 under iron-limiting conditions, can improve photosynthetic activity and cell growth. Transformed *P. tricornutum* strains were obtained expressing a single-mutant of the plastocyanin from the green algae *Chlamydomonas reinhardtii* that had previously shown to be the more effective in reducing *P. tricornutum* photosystem I *in vitro*. Our results indicate that even the relatively low intracellular concentrations of holo-plastocyanin detected (≈4 µM) are enough to promote an increased growth (up to 60%) under iron-deficient conditions as compared with the WT strain, measured as higher cell densities, content in pigments and active photosystem I, global photosynthetic rates per cell and even cell volume. In addition, the presence of plastocyanin as an additional photosynthetic electron carrier seems to decrease the over-reduction of the plastoquinone pool, and consequently promotes an improvement in the maximum quantum yield of both photosystem II and I, together with a decrease in the acceptor side photoinhibition of photosystem II –also associated to a reduced oxidative stress–, a decrease in the peroxidation of membrane lipids in the choroplast, and a lower degree of limitation on the donor side of photosystem I.

Abbreviations:

Cb_6f, cytochrome b_6f; Cc_{550}, cytochrome c_{550}; Cc_6, cytochrome c_6; Cf, cytochrome *f*; Chl, chlorophyll; ET, electron transfer; Fd, ferredoxin; Fld, flavodoxin; Pc, plastocyanin; PQ, plastoquinone; PSI, photosystem I; PSII, photosystem II; P_{700}, photosystem I primary donor; TL, STL and HTL, thermoluminescence, standard thermoluminescence and high temperature thermoluminescence, respectively; t_{max}, temperature of the maximum of a TL band; $t_{1/2}$, half-life time.

INTRODUCTION

Photosynthetic productivity, which is equally shared between terrestrial and oceanic systems, is due to a wide variety of organisms, from cyanobacteria to eukaryotic microalgae and plants (Hall 1976, Field et al. 1998). Within the group of eukaryotic microalgae, diatoms constitute the dominant life form in oceanic phytoplankton, probably representing the largest group of biomass producers on earth (Bowler et al. 2010).

The oxygenic photosynthetic electron transfer (ET) chain is composed by three large multisubunit membrane-embedded complexes, all of which contain iron cofactors: photosystem II (PSII), cytochrome b_6f (Cb_6f) and photosystem I (PSI), that are connected by mobile electron carriers (Blankenship 2014). In terrestrial plants, electrons from the Cb_6f complex are transferred to PSI inside the thylakoidal lumen by means of plastocyanin (Pc), a small (ca. 100 amino acids) soluble Type-1 blue copper-protein, whereas electrons from PSI are delivered to ferredoxin (Fd), an iron-sulphur protein. In aquatic systems however, many photosynthetic microorganisms maintain alternative electron transporters couples (Hervás et al. 2003). Thus, in most cyanobacteria and unicellular green algae, Pc is produced when copper is available, but under low-copper conditions Pc is replaced by cytochrome c_6 (Cc_6), a typical Class I *c*-type cytochrome (ca. 90 amino acids). By its turn, the flavoprotein flavodoxin (Fld) replaces Fd under iron-limiting conditions (Hervás et al. 2003, De la Rosa et al. 2006, Sancho 2006, Sétif 2006). The functional and structural equivalence of both couples, Pc/Cc_6 and Fd/Fld, is well established (Hervás et al. 1995, 2003, Hippler and Drepper 2006, Bendall and Howe 2016).

The existence of redox alternative couples in photosynthesis can be understood as an adaptation to fluctuations in the bioavailability of iron in the aquatic environments. Many studies have revealed that iron limitation is the major factor controlling the primary productivity and growth of phytoplankton in vast oceanic areas (Boyd et al. 2007, Moore and Braucher 2008). Massive oceanic iron fertilization experiments have also shown the appearance of algal blooms, in many cases dominated by diatoms, suggesting that these eukaryotic algae, in particular, are very sensitive to iron limitations (Morrissey and Bowler 2012). Among other effects, iron starvation causes a severe decrease in the chlorophyll content and drastic alterations in the photosynthetic efficiency in diatoms, promoting a decrease in the content of both the iron-rich PSI and Cb_6f complexes and resulting in an increased PSII:PSI ratio (Allen et al. 2008, Lommer et al. 2012, Marchetti et al. 2012).

However, the occurrence of alternative couples is only partially maintained in the red lineage of photosynthetic organisms, that diverged along evolution from the green lineage, and that comprises, among others, red algae, cryptophytes, stramenopiles (that include diatoms) and haptophytes (Falkowski et al. 2004). Thus, whereas Fld is widely produced in the red lineage as an alternative to Fd under low iron conditions (Pierella Karlusich et al. 2014), Cc_6 is the only electron carrier from cytochrome *f* (Cf) –in the Cb_6f complex– to PSI in red algae and in the majority of

organisms belonging to the red-plastid lineage, including diatoms, as confirmed by protein characterization, genome sequencing and transcriptomic analyses (Akazaki et al. 2009, Bowler et al. 2010, Blaby-Haas and Merchant 2012, Bernal-Bayard et al. 2013, Groussman et al. 2015). The absence of Pc as an alternative to Cc_6 can thus represent an extra requirement of iron that affects the adaption of these organisms to iron limitations, as Cc_6 replacement has been suggested to reduce iron requirements by up to 10% in open-ocean waters (Boyd et al. 2007, Guo et al. 2010). However, although *petJ* genes encoding Cc_6 have been found in all the sequenced stramenopiles genomes, *petE* genes encoding Pc, closely related to those from green algae, have been also found in the genomes of several strains of oceanic diatom species. These include *Thalassiosira oceanica* and *Fragilariopsis cylindrus*, but also the haptophyte *Emiliania huxleyi* and the dinoflagellate *Karenia brevis* (Nosenko et al. 2006, Peers and Price 2006, Blaby-Haas and Merchant 2012). In addition, analyses of microbial eukaryotic transcriptomes detected transcripts encoding for putative Pcs in at least one species from each of the major diatom classes (Groussman et al. 2015). All of this has been attributed to the acquisition of *petE* Pc genes from green alga by horizontal gene transfer, as an adaptation to iron limitation (Peers and Price 2006, Marchetti et al. 2012, Groussman et al. 2015, Hippmann et al. 2017). A particular strain of the open ocean diatom *T. oceanica* has been even described to express constitutively Pc as the main electron carrier from Cf to PSI, as the two Cc_6 genes of its genome are weakly expressed (Peers and Price 2006, Lommer et al. 2012, Kong and Price 2020). The presence of Pc in diatoms leaves, however, some open questions, such as the mechanism regulating either its expression or a putative Cc_6/Pc alternation in function of the copper/iron levels (Lommer et al. 2012, Marchetti et al. 2012, Roncel et al. 2016, Hippmann et al. 2017). In addition, the existence of a still not found specific transporting system carrying copper into the lumen, to be incorporated into the Pc, is another unresolved question (Levy et al. 2008, Guo et al. 2010, 2015, Kong and Price 2019).

Clear evidences for the production of a functional Pc protein have been only presented in the case of *T. oceanica*, where relatively small amounts per cell of the holoprotein were detected, purified and partially sequenced (Peers and Price 2006, Kong and Price 2020). However, there is a discordance between the theoretical molecular mass of the *T. oceanica* mature Pc (10,300 Da) and the apparent experimental mass found for the purified protein (18,200 Da) (Peers and Price 2006). In any case, the Pc-translated sequence in diatoms is closely related to that from green algae, and thus the "red-type" acquired Pc would show the features of a "green-type" Pc. In green algae (and plants) Pc two well-defined functional areas can be described: a hydrophobic ET area, determined by the accessibility to the solvent of the redox cofactor, and a strong negatively-charged area for the interaction with complementary positive patches in Cf and PSI, both features being also present in green Cc_6 (Guss and Freeman 1983, Ubbink et al. 1998, De la Rosa et al. 2006, Hippler and Drepper 2006). However, whereas Cc_6 from red algae and diatoms still preserves the hydrophobic ET area, it shows a significant decrease in the negative character of the electrostatic area (Yamada et al. 2000,

Akazaki et al. 2009, Bernal Bayard et al. 2013), parallel with equivalent changes in the electrostatics features of PSI (Bernal Bayard et al. 2013, 2015, Antoshvili et al. 2019) and Cf (Castell et al. unpublished data). Consequently, in vitro kinetic analyses of the interaction of diatom PSI with green algae and plants Pcs suggest that if an alternative Pc in diatoms could represent a favourable adaptation to iron limitation, its "green-type" character may however limit its ET efficiency. Remarkably, this efficiency increased in some green alga Pc mutants replacing negative charges for positive ones, in order to approximate to the electrostatics of diatom Cc_6 (Bernal-Bayard et al. 2015).

We have here investigated if the heterologous expression in the pennate model diatom *Phaeodactylum tricornutum* of a functional green alga Pc under iron-limiting conditions, as an alternative to Cc_6, can improve photosynthetic activity and cell growth. *P. tricornutum* is sensitive to iron limitation and both lacks Pc and produces Cc_6 (Allen et al. 2008, Akazaki et al. 2009, Bernal-Bayard et al. 2013). For this purpose, we have carried out the construction of *P. tricornutum* strains expressing a single-mutant of the Pc from the green algae *Chlamydomonas reinhardtii*, that has previously shown to be more effective than the WT Pc in reducing diatom PSI in vitro (Bernal-Bayard et al. 2015).

MATERIALS AND METHODS

Cell cultures

Cells from the coastal pennate diatom *Phaeodactylum tricornutum* CCAP 1055/1 were grown in artificial seawater (ASW) medium (McLachlan 1964, Goldman and McCarthy 1978) in a rotatory shaker (50 rpm) at 20ºC with regular transfer of the cells into fresh media. The cultures were illuminated by led white light (4500 K) lamps giving an intensity of 20 µmol m^{-2} s^{-1} (T8-150MWBL led lamps, Wellmax, China) following a light/dark cycle of 16/8 h. For the experiments to study the effects of iron deficiency, cells from cultures of 7 days were pelleted at 5000x*g* for 5 min and suspended and grown in fresh ASW medium under iron-replete (12 µM Fe) or iron-deficient (10 nM Fe plus 0.3 mg L^{-1} of copper) culture conditions, with transfer of the cells into the same fresh media after a week. Then, the cultures were grown for another 15 days. Except when indicated, most of the experiments were carried out using cultures with ≈6.5 x 10^7 cells mL^{-1} and ≈2 x 10^7 cells mL^{-1}, respectively, for iron-replete and iron-deficient conditions.

Plasmids construction

The nucleotide sequence of the WT Pc from the green alga *Chlamydomonas reinhardtii* was retrieved from the GenBank-NCBI database. A synthetic Pc *petE* gene, with the E85K mutation (Bernal-Bayard et al. 2015), was designed with the codon usage of *P. tricornutum* (https://www.kazusa.or.jp/codon/). Moreover, the Fld promoter (induced in the absence of iron) and the transit peptide of Cc_6 (directing the protein to the thylakoid lumen) of *P. tricornutum* were added upstream to the Pc-translated sequence. However, as the native Cc_6 gene of *P. tricornutum* has an intron (280 nucleotides) within the N-terminal plastid targeting sequence (Killian and Kroth 2004), two constructions with alternative versions of the transit peptide of Cc_6 were designed, with or without the sequence corresponding to the intron (Figure S1, Supplementary material). The synthetic plasmids were generated by GeneCust (Boynes, France), by inserting the Pc *petE* E85K constructions into pBlueScript II SK (+) vector in *Eco*RV and *Pst*I sites, and subcloned in the *P. tricornutum* transformation vector Isip1::YFP, kindly provided by the group of Prof. Chris Bowler (IBENS, Paris, France) (Kazamia et al. 2018), in the same restriction sites, to obtain the final pFld_PtCc6_PcE85K and pFld_PtVCc6_PcE85K plasmids (with and without the intron, respectively). Both plasmids were checked by sequencing (NZYTech), using the oligonucleotides pPisipF (5'-TCTCGTGTGGTCATGGGTTG-3') and pPisipR (5'-ACGACTTCTTCAAGTCCGCC-3'). To obtain antibodies against the Fld from *P. tricornutum*, the *FLDA1* gene coding for Fld was amplified by PCR from genomic DNA, using the iProof™ High-Fidelity DNA Polymerase (Bio-Rad) and adequate oligonucleotides, and the PCR product was cloned into the pET-28 b (+) vector (Novagen), to obtain the pET-28 b_Fld plasmid for expressing the His-tagged protein in *E. coli.* All

plasmids were maintained in the *E. coli* DH5α strain (Hanahan 1983), isolated when required as described by Ish-Horowicz and Burke (1981) and quantified using a NanoDrop N-1000 spectrophotometer.

Cell transformation by biolistic

P. tricornutum cells were transformed using the Biolistic PDS-1000/He Particle Delivery System (Bio-Rad) as previously described (Apt et al. 1996, Falciatore et al. 1999). Approximately 5 x 10^7 cells, harvested at mid-logarithmic phase, were spread on ASW, 1% (w/v) agar plates and incubated for 24 h. M17 tungsten microcarrier particles (1.1 µm diameter) (Bio-Rad) were coated with plasmid DNA using $CaCl_2$ and spermidine as indicated by the supplier. Agar plates were located at level two within the chamber and a burst pressure of 1550 psi was used for the bombardment. The cells were co-transformed with the pPha-T1 vector containing zeocin resistance, also kindly provided by the group of Prof. Chris Bowler. As a control of the possible effects of the zeocin resistance, an experiment in which *P. tricornutum* was transformed only with the zeocin resistance vector was also carried out (B1 mutants). Afterwards, the plates were incubated for 48 h in the dark before being spread onto new ASW agar plates containing 100 µg mL^{-1} of zeocin (InvivoGen), to allow the selection of transformants. Plates were then maintained under illumination with a light/dark cycle of 16/8 h at 20ºC as described above. Individual resistant colonies appearing 3–4 weeks after transformation were restreaked on new ASW agar plates containing zeocine. The presence of the Pc gene in zeocin-resistant colonies was checked by colony PCR, using the oligonucleotides pPisipF and pPisipR and the MyTaq™ Polymerase (Bioline), according to manufacturer's instructions. The amplified products were visualized through DNA electrophoresis in 0.7% (w/v) agarose gel (Sambrook and Russel 1989).

Analytical methods

Cells were counted with a Neubauer-Improved hemocytometer (Marienfeld-Superior), according to the manufacturer's instructions. Cell specific growth rate (µ, day^{-1}) was calculated after 15 days of culture growth as: [$\mu = \ln (N_t / N_0) / \Delta t$] where N_t and N_0 are the final and initial cell concentration, respectively, and Δt are the days of growth.

Pigments extraction with acetone was carried out basically as described by Kong and Price (2020), but with an initial step of incubation at 70ºC for 30 min. Chlorophyll *a* and *c* content in *P. tricornutum* cells was determined as described by Jeffrey and Humphrey (1975), whereas carotenoid concentration was determined by the equation given by Strickland and Parsons (1972):

Chl *a* (µg mL^{-1}) = 11.47 x ($A_{664} - A_{750}$) – 0.40 x ($A_{630} - A_{759}$)

Chl *c* (µg mL^{-1}) = 24.34 x ($A_{630} - A_{750}$) – 0.40 x ($A_{664} - A_{759}$)

Carotenoid (µg mL^{-1}) = 7.6 x (($A_{480} - A_{750}$) – 1.49 x ($A_{510} - A_{750}$))

For protein determination, *P. tricornutum* cells were pelleted and resuspended in 100–150 µL of lysis buffer [50 mM Tris-HCl, pH 7.5, buffer supplemented with 2% SDS, 10 mM EDTA and a tablet of the protease inhibitor cocktail (cOmplete™ ULTRA Tablets, EASYpack, Roche)]. The cells were incubated at 37ºC for 30 min with occasional vortexing. Soluble protein fractions were obtained by centrifugation at 15000x*g* for 30 min at 4ºC, and the protein concentration was determined according to the Lowry method (Lowry et al. 1951).

The Cc_6 and Pc E85K content in *P. tricornutum* cells were determined following a modification of the method previously described (Bernal-Bayard et al. 2017). *P. tricornutum* cells were collected by centrifugation. Wet pellets (≈3 g) were weighed and resuspended in 20 mL of 20 mM Tris buffer, pH 7.5, supplemented with DNase and the proteases inhibitors PMSF, benzamidine and aminocaproic acid. The cells were then broken by three cycles of French press disruption (20,000 psi), followed by debris precipitation with 55% ammonium sulfate and further precipitation with 100% ammonium sulfate. Cc_6 and Pc content were determined in the final resuspended pellets by differential absorbance measurements between the fully reduced (sodium ascorbate) and fully oxidized (potassium ferricyanide) states, at 552 nm (Cc_6, reduced minus oxidized) or 600 nm (Pc, oxidized minus reduced), as previously described (Bernal-Bayard et al. 2015, Roncel et al. 2016). To reduce interferences from Cc_6 absorbance in the determination of Pc, the concentration of Cc_6 was first determined and an equivalent concentration of purified Cc_6 was used as baseline to measure Pc concentration more precisely. *P. tricornutum* Fld purification was carried out by FPLC (IBVF Chromatography Service) using a HisTrap Fast Flow Crude column (GE Healthcare Life Sciences) from the inclusion bodies of *E. coli* BL21 (DE3) cells transformed with pET-28 b_Fld, after IPTG induction in the presence of 10 µM FMN and by following, with some modifications, protocols previously described (Purifying Challenging Proteins Handbook from GE Healthcare, and see also Rogl et al. 1998). MALDI-TOF mass spectrometry (IBVF Proteomic Service) was used to confirm the correct molecular weight of the purified protein.

Western-blot analysis

For the immunodetection of *C. reinhardtii* Pc and *P. tricornutum* Cc_6, cytochrome c_{550} (Cc_{550}) and Fld, polyclonal antibodies raised against those proteins were generated using standard procedures at the Animal Experimentation Facility (University of Seville, Spain) by subcutaneous injection of 1 mg of the purified proteins into a white New Zealand rabbit (Bernal-Bayard et al. 2013, 2015, 2017). Commercial antibodies against D1 and PsbO proteins were obtained from Agrisera (Vännäs, Sweden), whereas antibodies against PsaB were kindly provided by Dr. Anna Lindahl (IBVF, Sevilla, Spain).

Protein extracts (2.5-30 µg) were resolved on 15% (w/v) polyacrylamide gel electrophoresis, as previously described (Roncel et al. 2016), and transferred to a 0.2 µm nitrocellulose membrane included in the Trans-Blot® Turbo™ RTA Midi Nitrocellulose Transfer Kit through the Trans-Blot®

Turbo™ Transfer System (Bio-Rad), following the manufacturer's instructions. The membrane was incubated overnight with a dilution (1:500 to 1:10000) of the selected primary antibody followed by 1 h incubation with a 1:10000 dilution of the secondary antibody (Goat Anti-Rabbit IgG (H+L)-HRP Conjugate) (Bio-Rad). Finally, the membrane was treated with the Immobilon Western Chemiluminescent HRP Substrate (Millipore) according to the manufacturer's instructions, and visualized with the ChemiDoc™ Imaging System (Bio-Rad).

Microscopy

To monitor the Pc expression and localization in *P. tricornutum* transformed strains, as well as cell morphology of the different strains, cells were observed and photographed using a Leica Microscope DM6000 B apparatus (Leica Microsystem) (IBVF Microscopy Service). The immunostaining and fluorescence microscopy was carried out following the protocol previously described in Szabo and Colman (2007), with some modifications. Cells were extended in a slide and fixed, incubated with rabbit polyclonal anti-Pc antibody, washed, incubated with anti-rabbit FITC secondary antibody (Sigma), washed again and mounted.

The morphology of WT and transformed cells of *P. tricornutum*, grown under iron-replete or iron-deficient conditions, was imaged in vivo also by fluorescence microscopy. Cell volumes and surfaces were calculated from images measurements of longitudinal and transversal cell dimensions and treating *P. tricornutum* as a two cones model (Levy et al. 2008). In addition, cells aspect ratio ([Major Axis]/[Minor Axis]) and circularity (4π x ([Area]/[Perimeter]^2)) shape descriptors were estimated according the ImageJ Fiji software (v. 1.46) (Schindelin et al. 2012).

Thermoluminescence analyses

Thermoluminescence (TL) glow curves of *P. tricornutum* cell suspensions were obtained using a home-built apparatus designed by Dr. Jean-Marc Ducruet for luminescence detection from 1ºC to 80ºC (standard thermoluminescence, STL) and from 10ºC to 160ºC (high temperature thermoluminescence, HTL). A detailed description of the system can be obtained elsewhere (Roncel et al. 2016, García-Calderón et al. 2019). Temperature regulation, signal recording and flash sequences were driven by a computer through a National Instrument DAQ-Pad1200 interface, using a specific acquisition program developed by Dr. Ducruet. An electrically insulated resistor heater (Thermocoax), powered by a variable (0 to 5 A) computer-driven power supply, was mounted below the chamber for temperature regulation. STL and HTL measurements were carried out basically as described in Roncel et al. (2016). Most of the experiments were carried out using cultures with a cellular concentration of ≈1.5 x 10^8 and ≈5 x 10^7 cells mL^{-1} for TL and HTL, respectively.

Photosynthetic measurements

To study photosynthetic global activity, cells from 2.5 mL of the different cultures were collected by centrifugation and resuspended in fresh culture medium. Oxygen intake or evolution were then determined by using a Clark-type oxygen electrode (Hansatech) at 20°C, both in the dark and under illumination (176 µmol m^{-2} s^{-1}), to establish the net photosynthetic activity per cell.

The chlorophyll *a* fluorescence of PSII and the redox state of P_{700} from intact cells were determined at room temperature using a pulse-amplitude modulation fluorometer (DUAL-PAM-100, Walz, Effeltrich, Germany). Experiments were carried out on whole cells basically as described in Roncel et al. (2016). Prior to measurements, cell suspensions with a cellular concentration of 1.1 x 10^8 cells mL^{-1} were dark adapted for 30 min. The maximum quantum yield of PSII (F_v/F_m), the relative linear electron transport rates (rETR) and the effective PSII quantum yield [Y(II)], for each actinic light intensity were determined as previously described (Roncel et al. 2016).

The redox sate of P_{700} was monitored by following changes in absorbance at 830 nm versus 875 nm in cells dark-adapted for 30 min prior to measurements. Most of the experiments were carried out using cultures with a cellular concentration of ≈5.5 x 10^7 and ≈4.5 x 10^8 cells mL^{-1} for iron-replete and iron-deficient cultures, respectively. The level of maximal P_{700}^+ signal observed upon P_{700} full oxidation, P_m, was determined by illumination of cell suspensions with FR light (730 nm) for 10 s and thereafter with a saturating pulse of red light (635 nm) at 10000 µmol m^{-2} s^{-1} intensity and 0.6 s duration. Following P_m determinations, P_{700}^+ reduction kinetic decays were recorded in darkness. Averages of at least three individual traces were taken. The half-life time ($t_{1/2}$) of the P_{700}^+ absorption decay was determined by fitting the decays to a single exponential function. The quantum yields of PSI photochemistry, Y(I), donor side limitations, Y(ND), and acceptor side limitations, Y(NA), were determined as described in Roncel et al. (2016).

RESULTS

The expression of Pc in some oceanic species of diatoms has been proposed to constitute an alternative replacement of Cc_6, similar to what occurs in cyanobacteria and green algae (Peers and Price 2006, Moore and Braucher 2008, Lommer et al. 2012, Marchetti et al. 2012, Groussman et al. 2015, Hippmann et al. 2017). However, there are not available data about the in vivo specific functional effects of expressing Pc in the thylakoidal lumen of diatoms under iron limiting conditions. Thus, here we have investigated the effects of the heterologous expression of a Pc in *P. tricornutum*, a diatom that naturally only produces Cc_6. We have selected the E85K single-mutant of the Pc from the green alga *C. reinhardtii* to be expressed in *P. tricornutum*, as this mutant has previously shown to be the more effective Pc in reducing diatom PSI in vitro (Bernal-Bayard et al. 2015). The *C. reinhardtii* E85K Pc gene was placed under the control of the Fld promoter, to ensure its expression in low iron conditions (Figure 1A), in which the levels of native Cc_6 drastically decrease and become limiting for the photosynthetic activity (Roncel et al. 2016, and see below). The tripartite transit peptide of the native Cc_6 was added to the Pc gene sequence, to warrant the transit of the protein to the thylakoid lumen (Killian and Kroth 2004). As the native Cc_6 gene of *P. tricornutum* has an intron (280 nucleotides) located within the region coding for the N-terminal plastid targeting sequence (Killian and Kroth 2004), a version of the transit peptide of Cc_6 without the sequence corresponding to the intron was also alternatively used (Figure S1, Supplementary material).

The presence of the Pc gene in zeocin-resistant transformed colonies was checked by colony PCR and DNA electrophoresis in agarose gels (not shown). The nuclear transformation of *P. tricornutum* is basically random, which can result in a great variability in the expression of a protein in different clones. Consequently, several *P. tricornutum* strains with different levels of Pc expression were selected (clones #30, #45 and #79), as shown by the presence in western-blot analysis of a band corresponding to the expected size of Pc (10.2 kDa; Figure 1A) and with the following apparent progression in the levels of expression: #30 < #45 < #79. Whereas mutants #30 and #45 were transformed with the construction that contained the intron in the plastid targeting gene sequence, mutant #79 lacked the intron (Figure S1, Supplementary material), indicating that both constructions can be correctly processed. However, in the three mutant strains an additional band of an apparent higher size (12.6 kDa) was also observed (more abundant in the clone #79; Figure 1A), that can be tentatively assigned to unprocessed Pc molecules still containing the Cc_6 thylakoid transit peptide (24 extra amino acids; Killian and Kroth 2004) and that would be considered as apo-Pc. Fluorescence microscopy monitoring of immunolabelled cells confirmed the detection of the heterologous Pc in the chloroplast, as the green fluorescence associated to the immunodetection of Pc merged with the red fluorescence of photosynthetic pigments (not shown). Finally, the presence of the Pc holoprotein (i.e., with the copper active cofactor) was directly detected by its absorption spectrum in cell extracts (Figure 1B). From the recorded differential spectra, analogous amounts of

intracellular holo-Pc were estimated for mutants #45 (≈3.8 µM) and #79 (≈4.4 µM) (Figure 1B), whereas the lower levels of Pc detected in the mutant #30 did not allow obtaining a reliable estimate of the holo-protein content (not shown). On the other hand, a similar amount of ≈3.6 µM of intracellular Cc_6 was estimated for the WT and mutant strains under iron-deficient conditions according to specific spectral changes (not shown), which represents ≈12% of the concentration detected under iron-replete conditions (≈28 µM) (Bernal-Bayard et al. 2013).

It should be first noted that, under iron-replete conditions, the transformed strains did not show significant differences with the WT strain, nor did the B1 strain (with the resistance to zeocin but without Pc) both in iron-replete or iron-deficient conditions (not shown). However, the three selected transformed strains showed an increased cell growth under iron-deficient conditions as compared with the WT strain (Figures 1C and 2, upper). This increase was about 40% in the mutant #30, but up to 60% in the case of the #45 and #79 mutants (Figure 2 upper, and Table 1) although the growth of the three transformed strains was still sensibly lower as compared with iron-replete conditions (Figure 2, upper). Accordingly, the three transformed strains also showed higher values in the specific growth rate (µ, from 0.155 in the WT to 0.175-0.185 day^{-1} in the mutants), as well as in the total chlorophyll, chlorophyll *a* and *c* and carotenoid contents per mL as compared with WT cells under iron-deficient conditions (Table 1). Higher levels of pigments are still observed in the three mutants when chlorophyll content is normalized per cell, particularly in the mutants #45 and #79 (up to 40%; Table 1). Regarding global photosynthetic activity, the three transformed strains presented a significant enhancement in the net photosynthetic oxygen evolution normalized per cell as compared with the WT strain, with the higher values observed again for the #45 and #79 clones (Table 1).

Fluorescence microscopy analysis showed changes in cell morphology in the three mutant strains (Figure 2, lower, and Table 1). Thus, under iron-deficient conditions WT fusiform cells showed to be more elongated that in the mutant strains (aspect ratio of 6.52, 4.89, 4.25 and 5.15 for WT, #30, #45 and #79 cells, respectively). Consequently, the mutant strains also appeared with an increased circularity, which actually resulted in an increased cell volume (Table 1). Finally, chlorophyll auto-fluorescence indicated the presence in the mutant strains of chloroplasts with a shorter and thicker shape (Figure 2, lower).

The changes in the levels of some photosynthetic proteins under low iron conditions were visualized by western-blot analysis. In addition of Fld (used as a control of iron deficiency), the studied proteins included soluble Cc_6, PSII subunits (the intrinsic D1 subunit and the luminal extrinsic subunits cytochrome c_{550} –or Cc_{550}– and PsbO), as well as the intrinsic PsaB subunit of PSI. The deficiency of iron promotes a drastic decrease in the levels of the two luminal cytochromes, Cc_6 and Cc_{550}, more particularly in the case of Cc_6, as previously described at less drastic iron limitations (Roncel et al. 2016, Bernal-Bayard et al. 2017) (Figure 1A); western bands quantification allowed estimating a similar value of ≈10% in the levels of Cc_6 and ≈30% in Cc_{550} under iron deficient conditions in all the strains as compared with iron-replete conditions, in good agreement with the

spectroscopic measurements (see above). Regarding other PSII components, the levels of PsbO and D1 were basically analogous in the WT and mutant strains under iron deficiency (not shown). However, in the case of the PsaB subunit of PSI, the decrease observed in the WT strain (≈50%) under iron-deficient conditions seems to be partially recovered in the #45 and #79 mutant strains (Figure 1A). However, it is important to note that an increased production of PsaB does not necessarily imply an equivalent amount of active PSI, since other PSI iron-containing subunits are required in order to form functional PSI complexes (see below).

The effects of iron deficiency on PSII ET activity of *P. tricornutum* WT and mutant strains were investigated using the STL technique (Figure 3). Excitation of iron-deficient *P. tricornutum* WT cells with two flashes at 1ºC induced the appearance of a TL glow curve with significant differences in comparison with the curves obtained in iron-replete cells: a very significant decrease on the total TL signal intensity of about 65% (Figure 3, upper). The decomposition analysis of these emission curves allowed obtaining two components with similar t_{max} values of 14ºC and 28ºC for both iron conditions. These two components can be assigned to the well-known B1 and B2 TL bands originating from the recombination reactions of $S_3Q_B^-$ and $S_2Q_B^-$ charge pairs in PSII, respectively (Rutherford et al. 1984).

The TL glow curves obtained for the #79 (Figure 3, upper), #30 and #45 (not shown) mutant strains, could be also decomposed in two TL components, B1 and B2 bands. The t_{max} values for these components were similar to WT in all strains and for the two iron conditions. The TL glow curves obtained in iron-deficient conditions also showed a decrease in the total TL signal intensity with respect to iron-replete conditions (Figure 3). However, the decreases in intensity in the mutants were much lower in comparison with the WT strain: 39%, 56% and 18% for #30, #45 and #79 mutant strains, respectively.

The HTL technique was applied to detect lipid peroxidation in *P. tricornutum* WT and mutant cells cultured in both iron-replete and iron-deficient conditions. Figure 4 (upper) shows that a broad HTL2 band with maximum between 130-140°C was present in iron-deficient WT cells. This band was significantly lower in iron-replete cells. Thus, an important level of lipid peroxidation was observed in WT cells grown in iron-deficient conditions under the relatively low light intensity used. However, for the three mutant strains cultured under iron-deficient conditions, the level of lipid peroxidation was significantly lower (Figure 4).

Differences in the photosynthetic activity of PSII between iron-replete and iron-deficient WT cells have been already described (Roncel et al. 2016). Thus, the effects of iron deficiency on PSII photochemistry in the mutants expressing Pc have been here investigated by chlorophyll *a* fluorescence measurements. Thus, the maximum quantum yield of PSII, F_v/F_m, was significantly decreased in iron-deficient WT cells (F_v/F_m = 0.331) in comparison with iron-replete cultures (F_v/F_m = 0.632) (Table 2). However, the three mutants showed a partial recovery (≈15-30%) of the F_v/F_m

values as compared to WT cells under conditions of iron deficiency, with higher values being obtained for the #45 (0.384) and #79 mutants (0.425) (Table 2).

It has been shown previously that PSII light saturation curves, carried out in cultures of *P. tricornutum* under iron-replete and iron-deficient conditions, showed differences in the relative electron transport rate (rETR), i.e., the ratio between absorbed light quanta and transported electrons, as well as in the light adaptation mechanisms (Roncel et al. 2016). In cells exposed to gradually increasing light intensities, the electron transport increases in parallel up to its limit capacity. Beyond this point, increasing light intensity induces photoinhibition, i.e., a decrease of the rETR. In this work, iron-deficient WT cells reached its maximum electron transport rate ($rETR_{max}$) at 150 μmol m^{-2} s^{-1}, showing a rETR almost completely inhibited at high light intensity (≈2000 μmol m^{-2} s^{-1}; Figure 5). In contrast, iron-replete WT cells have showed a $rETR_{max}$ of 500 μmol m^{-2} s^{-1} (Table 2). Under these conditions, the rETR value measured at the higher light intensity remained at about 70% of the maximum value (not shown). Therefore, these results confirmed a substantially higher sensitivity to light for *P. tricornutum* WT cells grown under low iron concentration (Roncel et al. 2016). In the case of the three selected transformed strains, PSII light saturation curves were performed in cultures under iron deficiency. Table 2 shows the higher values observed for the $rETR_{max}$ for the three mutants (reached at 200-350 μmol m^{-2} s^{-1}) as compared to that obtained in the WT (150 μmol m^{-2} s^{-1}) under the same conditions (Table 2). In addition, the three mutants showed higher rETR values at light intensities above 500 μmol m^{-2} s^{-1} and up to ≈2000 μmol m^{-2} s^{-1}, at which the rETR values still remained at about 12-40% of the maximum value, with higher values being observed again for the #45 and #79 mutants (Figure 5, and Table 2). These results suggest that under iron-deficiency, the three mutant strains exhibit better light tolerance, confirming the specific effect of expressing Pc in preventing earlier photoinhibition. This is also in line with the observed faster growth rate of the three mutants.

The effects of Pc expression on PSI activity under iron deficiency was also investigated by measuring the P_{700} redox state changes during illumination, as previously described (Roncel et al. 2016). In dark-adapted cultures, P_{700} is found reduced, since the acceptor side of P_{700}, i.e., the Calvin-Benson cycle and subsequent reactions, are deactivated. Under actinic light P_{700} is first oxidized and re-reduced by electrons coming from the plastoquinone (PQ) pool, and thus by applying saturating pulses its ability to become oxidized and re-reduced can be determined (Roncel et al. 2016). Induction-recovery curves were performed in iron-replete and iron-deficient cultures and, as shown in Figure 6A, the calculated quantum yield of PSI photochemistry, Y(I), increased in the three mutants as compared to WT cells under the same conditions of iron deficiency. On the other hand, the high degree of donor side limitations, Y(ND), observed in iron-deficient WT cells, was slightly reversed in all the mutants (Figure 6B).

The higher Y(I) of the three mutants seems to indicate a recovery of the PSI activity missing in the WT cells as a result of the lack of availability of electron donors for PSI (Roncel et al. 2016).

In contrast, similar acceptor-side limitations, Y(NA), were observed in all the cultures (Figure 6C). Thus, the presence of Pc in the three mutants seems to compensate for the deficiency in PSI activity by providing electrons to PSI in the light. To confirm this hypothesis, P_{700} reduction kinetics after saturating light pulses were recorded in iron-replete and iron-deficient conditions (not shown), in order to obtain the maximal P_{700}^{+} signal upon full oxidation (P_m) and the half-life time ($t_{1/2}$) parameters for P_{700}^{+} re-reduction (Table 2). Upon onset of the actinic light, P_{700} became quickly oxidized and reached a stable level of P_{700}^{+}. As expected, the P_m signal amplitude was significantly lower in WT iron-deficient cells in comparison with iron-replete conditions (Table 2). Under conditions of iron deficiency, the three mutants exhibited, however, a slightly higher P_m signal compared to WT cells, thus indicating a higher amount of active P_{700} (Table 2). After turning off the actinic light, the P_{700}^{+} reduction takes place in darkness and $t_{1/2}$ for the P_{700}^{+} absorption decay can be calculated (Table 2). Thus, the value of $t_{1/2}$ in WT iron-deficient cultures was ≈3 times higher as compared with iron-replete conditions (11.82 *versus* 4.45 ms; Table 2). However, under iron deficiency, $t_{1/2}$ values were ≈2 times lower in the three mutants in comparison with WT cells (≈5.8 ms) (Table 2), thus indicating an acceleration of P_{700}^{+} re-reduction in the three mutants as compared with iron-deficient WT cells (Table 2).

DISCUSSION

Adaptations of diatoms to natural oceanic low-iron environments include, among other effects, the induction of iron-uptake systems and the lowering of iron-containing photosynthetic proteins, in particular Fd (replaced by Fld) and the PSI and Cb_6f complexes, thus decreasing iron requirements (Strzepek and Harrison 2004, Lommer et al. 2012). In addition, the presence of *petE* Pc genes in the genomes of some oceanic diatoms has been explained by their acquisition from green alga by horizontal gene transfer, as an adaptation to chronic iron limitations in these environments (iron concentration <1 nM) (Moore and Braucher 2008). Thus, Pc acquisition and expression in oceanic diatoms has been considered to represent an alternative (or even constitutive) substitution of Cc_6, as it occurs in cyanobacteria and green algae (Peers and Price 2006, Moore and Braucher 2008, Lommer et al. 2012, Marchetti et al. 2012, Groussman et al. 2015, Hippmann et al. 2017). An open question is the mechanism regulating a putative Cc_6/Pc replacement in diatoms. In cyanobacteria and green algae, are the copper levels that determine the expression of one protein or another (Merchant and Bogorad 1986, Sandmann 1986, Kropat et al. 2005), but in diatoms both low copper and sufficient iron conditions have been reported to induce a decrease in Pc transcripts which, on the contrary, can be detected under iron limiting conditions (Lommer et al. 2012, Marchetti et al. 2012, Hippmann et al. 2017, Rizkallah et al. 2020). Recently, a 3-fold decrease in the Pc protein content under copper deficiency has been reported in *T. oceanica* (Kong and Price 2020), in contrast to the drastic changes in Pc content in response to changes in copper concentration observed in cyanobacteria and green algae (Merchant and Bogorad 1986, Sandmann 1986, Durán et al. 2005). By its turn, our results indicate that Cc_6 levels in *P. tricornutum* depend on the availability of iron (Roncel et al. 2016), although iron uptake itself is connected to copper availability (Maldonado et al. 2006).

Although a Pc holoprotein was purified from *T. oceanica* (Peers and Price 2006), this protein has not been fully characterized nor its cloning and expression in *Escherichia coli* has been achieved. Therefore, there are not functional data available for the interaction of the “red” partners (PSI or Cf) with the "green-type" Pc acquired by horizontal gene transfer. However, in vitro kinetic analysis of the interaction of *P. tricornutum* PSI with green algae and plants Pc indicated that diatom PSI is able to react with the very acidic Pc from these organisms, although with lower efficiency than with *P. tricornutum* Cc_6. Moreover, in the *C. reinhardtii* E85K Pc mutant, designed trying to mimic the electrostatics of diatom Cc_6, this efficiency doubled as compared with the WT protein (Bernal-Bayard et al. 2015).

The estimated holo-Pc concentration per cell in *T. oceanica* under copper sufficient conditions (≈3 μM) is however about 10 times lower than that usually described for Cc_6 under iron sufficient conditions, including reported values in the coastal *P. tricornutum* diatom (≈28 μM) (Peers and Price 2006, Bernal-Bayard et al. 2013, Kong and Price 2020). Pc levels in *T. oceanica* are, however,

comparable to the Cc_6 content found under iron-deficient conditions in *P. tricornutum* (≈4-7 μM) (see above, and Roncel et al. 2016) and, interestingly, to the levels of heterologous holo-Pc here detected (≈4 μM). In this sense, although copper uptake systems have been described in *T. oceanica* (Kong and Price 2019), the functional expression of Pc requires a specific copper-transporting system into the thylakoid that has not yet been found in red-type organisms, including chaperones for copper traffic and, in particular, a P-type ATPase transporter located in the thylakoid membrane, delivering copper to the lumen to be incorporated into Pc (Guo et al. 2010, 2015, Nouet et al. 2011, Blaby-Haas and Merchant 2012, Kong and Price 2019). Thus is possible that, in the absence of specific mechanisms of copper import, the limitation in the copper available in the lumen to be incorporated into Pc restrains the amount of a functional holoprotein to the levels described in *T. oceanica* and found in this work (Ho et al. 2003, Levy et al. 2008, Twining and Baines 2013). However, our results indicate that even the relatively low concentrations of holo-Pc detected are enough to promote an increased growth (up to 60% in the case of the #45 and #79 mutants) under iron-deficient conditions as compared with the WT strain (Figure 2), measured as higher cell densities, content in pigments (chlorophylls and carotenoids) and active PSI, global photosynthetic rates per cell and even cell volume (Table 1). In addition, the Pc-expressing strains show changes in cell morphology that indeed reflect changes in the physiological and metabolic status of cells. *P. tricornutum* is a pleiomorphic diatom, although under normal laboratory culturing conditions the fusiform morphotype largely predominates (Martin-Jézéquel and Tesson 2012). However, the fusiform type can have different shapes depending of growth conditions. Thus, under iron limitation fusiform morphotype was shown to decrease in cell diameter and cell volume, whereas high copper concentrations induced the presence of cells with a shorter, swollen shape (Levy et al. 2008, Martin-Jézéquel and Tesson 2012). In our case, the Pc-expressing mutants show specific morphological features, as the presence of less-elongated fusiform cells with a decreased aspect ratio, an increased circularity and chloroplasts with a shorter and thicker shape (Figure 2).

In addition, PSII activity of *P. tricornutum* cells was affected by low iron concentration in a different manner in the WT and mutant strains. The decreased PSII activity in iron-deficient conditions detected by TL experiments (Figure 3) may be attributed to a reduced amount of functional PSII complexes in cells (Msilini et al. 2011). The partial blocking of ET between PSII and PSI in cells cultured under iron-deficient conditions can generate the over-reduction of the PQ pool. Under iron-deficient conditions, P_{700} cannot become reduced, possibly due to fewer available iron-containing ET proteins downstream of the PQ pool, such as the Cb_6f complex or the Cc_6 soluble donor (Bruce and Malkin 1991, Greene et al. 1992, Allen et al. 2008, Roncel et al. 2016). In particular, in *P. tricornutum* cells grown under low iron conditions, the Cc_6 concentration is reduced to ≈10-12% of the protein present in iron-replete cells, thus presumably disfavouring the PQ pool re-oxidation (Roncel et al. 2016). An over-reduction of the PQ pool may induce the appearance of the acceptor side photoinhibition process, that can decrease PSII activity. The existence of an alternative

electron carrier in the mutant strains, the E85K Pc, could improve the ET to PSI, and partially eliminate the over-reduction of the PQ pool and the concomitant lack of activity of PSII. This hypothesis can explain the significant lower decrease of the TL intensity signal in the WT strain (Figure 3) as well as the higher maximum quantum yield of PSII obtained by fluorescence measurements in the mutants compared to the WT (Table 2). Higher values for $rETR_{max}$ were also determined in the three mutants with respect to the WT (Figure 5, Table 2), which indicates that the aforementioned occurrence of the acceptor side photoinhibition process is delayed due to the presence of Pc.

A consequence of the acceptor side photoinhibition in PSII is the generation of singlet oxygen species (Murata et al. 2007). The formation of singlet oxygen can initiate the peroxidation of unsaturated lipids in membranes (Vavilin and Ducruet 1998). The level of lipid peroxidation in photosynthetic membranes can be measured by the HTL technique (Roncel et al. 2007). Several luminescence high temperature bands (HTL bands) have been observed without prior illumination at temperatures above 60°C (Ducruet and Vavilin 1999, Roncel et al. 2007). A broad HTL band centred near 130°C (known as the HTL2 band) is generated because of the thermal radiative decomposition of lipid peroxides that, in turn, leads to the formation of carbonyl groups in a triplet state followed by migration of excitation energy toward chlorophylls (Vavilin and Ducruet 1998, Ducruet and Vavilin 1999, Vavilin et al. 2002). The amplitude of this band has been well correlated with the accumulation of malondialdehyde, an indicator of lipid peroxidation in standard chemical tests (Vavilin and Ducruet 1998, Vavilin et al. 2002).

Analysis of HTL2 bands of TL obtained in *P. tricornutum* cells (Figure 4) clearly showed a much higher level of lipid peroxidation in iron-deficient conditions in the WT strain. However, in the three mutant strains the level of peroxidation did not significantly increase under iron-restricted conditions. These results suggest a higher rate of generation of reactive singlet oxygen under iron-deficient conditions in the WT strain. As previously said, the low levels of Cc_6 probably induce the over-reduction of the PQ pool and the concomitant acceptor side photoinhibition in PSII, and thus singlet oxygen production. The existence of Pc in the mutant strains under iron-deficient conditions could partially eliminate the over-reduction of the PQ pool and the concomitant generation of singlet oxygen, thus decreasing oxidative stress and lipid peroxidation.

On the other hand, it has been shown that PSI activity is more sensitive than PSII activity to iron-limitation (Pushnik and Miller 1989, Roncel et al. 2016). The significant decrease in the quantum yield of PSI, Y(I), observed in iron-deficient WT cells (Figure 6) can be ascribed to a deficiency of PSI donors, which causes that P_{700} cannot become reduced (Bruce and Malkin 1991, Greene et al. 1992, Allen et al. 2008, Roncel et al. 2016). An increase of Y(I) and a lower degree of limitation on the donor side of PSI, Y(ND), have been here observed in the three mutants (Figure 6A-B). The existence of Pc as an additional electron carrier in the mutant strains seems to improve

ET to PSI and, consequently, to partially increase Y(I), as well as to decrease the over-reduction of the PQ pool and the concomitant donor-side limitation of PSI.

In summary, our results show that the presence of Pc as an additional electron carrier in *P. tricornutum* under iron-limiting conditions seems to decrease the over-reduction of the PQ pool, and consequently promotes an improvement in the maximum quantum yield of both PSII and PSI, together with a decrease in the acceptor side photoinhibition of PSII and oxidative stress, the peroxidation of lipids and a lower degree of limitation on the donor side of PSI. Consequently, the mutants expressing Pc in *P. tricornutum* exhibit an enhancement in cell growth under iron limiting conditions as compared to WT cells.

FIGURE LEGENDS:

Figure 1. (A) Western blot analysis of different photosynthetic proteins in samples from *P. tricornutum* WT and #30, #45 and #79 mutant cells under iron-deficient conditions. MW, molecular weight standard; WT+ and WT–, control WT cells under iron-replete or iron-deficient conditions, respectively; Pc, E85K plastocyanin; Fld, flavodoxin; Cc_6, soluble cytochrome c_6; Cc_{550}, the extrinsic cytochrome c_{550} subunit of PSII; PsaB, the membrane intrinsic subunit of PSI. Protein extracts: 30 µg Pc; 20 µg PsaB; 10 µg Cc_6; 5 µg Fld; 2.5 µg Cc_{550}. Membranes were incubated overnight with the following dilutions of the selected primary antibody: 1:500 anti-Pc; 1:1000 anti-Cc_6, Cc_{550} and PsaB; 1:50000 anti-Fld. (B) Spectroscopic monitoring of holo-Pc (ferricyanide minus ascorbate) in cell extracts from mutant #45 under iron-deficient conditions. (C) Examples of WT and mutant #45 individual cultures under iron-replete (+) or iron-deficient (–) conditions.

Figure 2. (*Upper, left*) Growth of *P. tricornutum* WT cultures under iron-replete (+Fe) or iron-deficient (–Fe) conditions. (*Upper, right*) Growth of WT, #30, #45 and #79 strains cultures under iron-deficient conditions. Growth points are the mean values of 10 independent cultures. (*Lower*) Microscopy images of (*left*) differential interference contrast or (*right*) chlorophyll auto-fluorescence of *P. tricornutum* fusiform cells from cultures of the WT and #45 strains under iron-deficient conditions. Black bars indicate a 5 µm scale. See Material and Methods section for more details.

Figure 3. Effects of iron deficiency on the PSII activity of *P. tricornutum* cells measured by the STL technique. (*Upper*) Standard TL glow curves of the WT and #79 strains for iron-deficient (–Fe) and iron-replete (+Fe) conditions, as indicated. The Figures shown are representative examples. (*Lower*) Intensities of TL B1 and B2 bands for all the strains investigated under iron-replete (+) or iron-deficient (–) conditions, as indicated. Intensities were obtained from the component analysis of the curves of TL. Data represent mean values ± SD. See the Materials and Methods section for further technical details.

Figure 4. Effects of iron deficiency on the lipid peroxidation of *P. tricornutum* WT and mutant strains measured by the HTL technique. (*Upper*) High temperature TL glow curves (HTL2 band) of WT and #79 mutant strains for iron-replete (+Fe) or iron-deficient (–Fe) conditions, as indicated. The Figures shown are representative examples. (*Lower*) Intensities of HTL2 bands for all the strains investigated under iron-replete (+) or iron-deficient (–) conditions, as indicated. Intensities were obtained from the component analysis of the curves of HTL. See the Materials and Methods section for further technical details.

Figure 5. Relative linear electron transport rate (rETR) in the WT and #30, #45 and #79 mutant strains of *P. tricornutum* cells under iron deficiency, as indicated. rETR values were determined as a function of irradiance derived from steady-state light curves. Chlorophyll fluorescence was measured with a pulse-amplitude modulation fluorometer and rETR values were determined during stepwise increasing photosynthetically active radiation (PAR) from 0 up to 1956 μmol m^{-2} s^{-1} light intensity. Data represent the mean ± SD of five independent experiments.

Figure 6. (A-C) PSI activity of WT (WT –Fe) and #30, #45 and #79 mutant cells of *P. tricornutum* under iron deficiency, as indicated. Values of WT cells in iron-replete conditions (WT +Fe) are also included as a control. The redox state of the PSI reaction centre, P_{700}, was monitored through the changes in absorbance at 830 nm versus 875 nm, measured with a pulse-amplitude modulation fluorometer. Cultures of the different strains were kept in the dark for 30 min prior to the measurements. After the initial determination of the maximal oxidation of P_{700}, actinic light was turned on at an intensity of 430 μmol m^{-2} s^{-1} and saturating pulses were applied every 20 s. After 5 min the actinic light was switched off and measurements were continued for another 5 min. Changes of (A) quantum yields of PSI, Y(I), (B) donor side limitations, Y(ND), and (C) acceptor side limitations, Y(NA), during the course of the induction curve are displayed. White and black bars below graphs indicate periods of illumination with actinic light and darkness, respectively. Data represent the mean of five independent experiments.

Supporting information

Aditional supporting information is available in the online version of this article:

Appendix Figure S1. Genetics constructions used to transform *P. tricornutum* cells.

Data availability statement

The data that support the findings of this study are available from the corresponding author upon reasonable request.

Author contributions.

JAN and MH conceived and designed the project. CC and PB-B carried out the molecular biology genetic work as well as cells transformation and selection. CC, with the help of JAN and MH, carried out the physiological and biochemical characterization of the different strains here studied. MR and CC carried out PAM experiments and JMO and CC the TL measurements. All the authors discussed the results and JAN wrote the manuscript with their collaboration. The manuscript was corrected, revised and approved by all authors.

Acknowledgements

This article is dedicated to the memory of Jean-Marc Ducruet, to whom we will always be grateful for his support in the installation of thermoluminescence technology at the IBVF in Seville. This work was partially supported by the Spanish Ministry of Economy, Industry and Competitiveness (BIO2015-64169-P) and the Andalusian Government (PAIDI BIO-022). These grants were partially financed by the EU FEDER Program. C. Castell is the recipient of a FPU Program fellowship (Spanish Ministry of Education, Culture and Sports). The authors thank Dr. A. Orea (Microscopy Service, IBVF) for her technical assistance, Dr. Vicente Mariscal by his help in the immunolabelling microscopy experiments, Dr J. Paz and Prof. C. Bowler (IBENS, Paris, France) for kindly providing us with the Isip1::YFP and pPha-T1 plasmids and the group of *Biotecnología de semillas* (IRNAS, Sevilla, Spain) for the use of their Biolistic system.

References

Akazaki H, Kawai F, Hosokawa M, Hama T, Chida H, Hirano T, Lim B-K, Sakurai N, Hakamata W, Park S-Y, Nishio T, Oku T (2009) Crystallization and structural analysis of cytochrome c_6 from the diatom *Phaeodactylum tricornutum* at 1.5 Å resolution. Biosci Biotechnol Biochem 73:189–191

Allen AE, Laroche J, Maheswari U, Lommer M, Schauer N, Lopez PJ, Finazzi G, Fernie AR, Bowler C (2008) Whole-cell response of the pennate diatom *Phaeodactylum tricornutum* to iron starvation. Proc Natl Acad Sci USA 105 (30):10438–10443

Antoshvili M, Caspy I, Hippler M, Nelson N (2019) Structure and function of photosystem I in *Cyanidioschyzon merolae.* Photosynthesis Research 139:499–508

Apt KE, Grossman AR, Kroth-Pancic PG (1996) Stable nuclear transformation of the diatom *Phaeodactylum tricornutum*. Mol Gen Genet 252:572–579

Bendall DS, Howe CJ. The interaction between cytochrome *f* and plastocyanin or cytochrome c_6. In: (Cramer WA and Kallas, eds.) Cytochrome Complexes: Evolution, Structures, Energy Transduction, and Signaling. Advances in Photosynthesis and Respiration 41, pp. 631-655. Springer Science + Business Media, Dordrecht 2016

Bernal-Bayard P, Molina-Heredia FP, Hervás M, Navarro JA (2013) Photosystem I reduction in diatoms: as complex as the green lineage systems but less efficient. Biochemistry 52:8687−8695

Bernal-Bayard P, Pallara C, Castell C, Molina-Heredia FP, Fernández-Recio J, Hervás M, Navarro JA (2015) Interaction of photosystem I from *Phaeodactylum tricornutum* with plastocyanins as compared with its native cytochrome c_6: reunion with a lost donor. Biochim Biophys Acta Bioenerg 1847:1549–1559

Bernal-Bayard P, Puerto-Galán L, Yruela I, García-Rubio I, Castell C, Ortega JM, Alonso PJ, Roncel M, Martínez JI, Hervás M, Navarro JA (2017) The photosynthetic cytochrome c_{550} from the diatom *Phaeodactylum tricornutum*. Photosynth Res 133:273–287

Blaby-Haas CE, Merchant SS (2012) The ins and outs of algal metal transport. Biochim Biophys Acta 1823:1531–1552

Blankenship RE. Molecular Mechanisms of Photosynthesis, 2nd Edition. Wiley-Blackwell 2014

Bowler C, Vardi A, Allen AE (2010) Oceanographic and biogeochemical insights from diatom genomes. Annu Rev Marine Sci 2:333–365

Boyd PW, Jickells T, Law CS et al (2007) Mesoscale iron enrichment experiments 1993-2005: synthesis and future directions. Science 315:612–617

Bruce BD, Malkin R (1991) Biosynthesis of the chloroplast cytochrome b_6f complex: studies in a photosynthetic mutant of *Lemna*. The Plant Cell 3:203–212

De la Rosa MA, Molina-Heredia FP, Hervás M, Navarro JA. Convergent evolution of cytochrome c_6 and plastocyanin. The evolutionary pathways of the two proteins are connected to the geochemical changes in iron and copper availabilities. In: (Golbeck JH, ed.) Photosystem I: the Ligth Driven Plastocyanin:Ferredoxin Oxidoreductase. Advances in Photosynthesis and Respiration 24, pp. 683–696. Springer, Dordrecht, The Netherlands 2006

Ducruet JM, Vavilin D (1999) Chlorophyll high-temperature thermoluminescence emission as an indicator of oxidative stress: perturbating effects of oxygen and leaf water content. Free Radic Res 31 Suppl:S187–192

Durán RV, Hervás M, De la Rosa MA, Navarro JA (2005) *In vivo* photosystem I reduction in thermophilic and mesophilic cyanobacteria: The thermal resistance of the process is limited by factors other than the unfolding of the partners. Biochem Biophys Res Commun 334:170–175

Falciatore A, Casotti R, Leblanc C, Abrescia C, Bowler C. (1999) Transformation of nonselectable reporter genes in marine diatoms. Mar Biotechnol 1(3):239–251

Falkowski PG, Katz ME, Knoll AH, Quigg A, Raven JA, Schofield O, Taylor FJ (2004) The evolution of modern eukaryotic phytoplankton. Science 305(5682):354–360

Field CB, Behrenfeld MJ, Randerson JT, Falkowski P (1998) Primary production of the biosphere: integrating terrestrial and oceanic components. Science. 281(5374):237–240

Franklin NM, Stauber JL, Lim RP (2001) Development of flow cytometry-based algal bioassays for assessing toxicity of copper in natural waters. Environ Toxicol Chem 20:160–170

García-Calderón M, Betti M, Márquez AJ, Ortega JM, Roncel M (2019) The afterglow thermoluminescence band as indicator of changes in the photorespiratory metabolism in the model legume *Lotus japonicus*. Physiol Plant 166:240–250

Goldman JC, McCarthy JJ (1978) Steady state growth and ammonium uptake of a fast-growing marine diatom. Limnol Oceanogr 23(4):695–703

Greene RM, Geider RJ, Kolber Z, Falkowski PG (1992) Iron-induced changes in light harvesting and photochemical energy conversion processes in eukaryotic marine algae. Plant Physiol 100(2):565–575

Groussman RD, Parker MS, Armbrust EV (2015) Diversity and evolutionary history of iron metabolism genes in diatoms. PLoS ONE 10:e0129081

Guo J, Annett AL, Taylor RL, Lapi S, Ruth TJ, Maldonado MT (2010) Copper-uptake kinetics of coastal and oceanic diatoms. J Phycol 46:1218–1228

Guo J, Green BR, Maldonado MT (2015) Sequence analysis and gene expression of potential components of copper transport and homeostasis in *Thalassiosira pseudonana*. Protist 166:58–77

Guss JM, Freeman HC (1983) Structure of oxidized poplar plastocyanin at 1.6 Å resolution. J Mol Biol 169:521–563

Hall DO (1976) Photobiological energy conversion. FEBS Letters 64:6–16

Hanahan D. (1983) Studies on transformation of *Escherichia coli* with plasmids. J Mol Biol 166(4):557–580

Hervás M, Navarro JA, De la Rosa MA (2003) Electron transfer between soluble proteins and membrane complexes in photosynthesis. Acc Chem Res 36:798–805

Hervás M, Navarro JA, Díaz A, Bottin H, De la Rosa MA (1995) Laser-flash kinetic analysis of the fast electron transfer from plastocyanin and cytochrome c_6 to photosystem I. Experimental evidence on the evolution of the reaction mechanism. Biochemistry 34:11321–11326

Hippler M, Drepper F. Electron transfer between photosystem I and plastocyanin or cytochrome c_6. In: (Golbeck JH, ed.) Photosystem I: the Ligth Driven Plastocyanin:Ferredoxin Oxidoreductase. Advances in Photosynthesis and Respiration 24, pp. 499–513. Springer, Dordrecht, The Netherlands 2006

Hippmann AA, Schuback N, Moon KM, McCrow JP, Allen AE, Foster LJ, Green BR, Maldonado MT (2017) Contrasting effects of copper limitation on the photosynthetic apparatus in two strains of the open ocean diatom *Thalassiosira oceanica*. PLoS One Aug 24;12(8):e0181753

Ho TY, Quigg A, Finkel ZV, Milligan AJ, Wyman K, Falkowski PG, Morel FMM (2003) The elemental composition of some marine phytoplankton. J Phycol 39:1145–1159

Ish-Horowicz D, Burke JF (1981) Rapid and efficient cosmid cloning. Nucleic Acids Res 9:2989–2998

Jeffrey S, Humphrey G (1975) New spectrophotometric equations for determining chlorophylls a, b, c1 and c2 in higher plants, algae and natural phytoplankton. Biochem Physiol Pflanz 167:191–194

Kazamia E, Sutak R, Paz-Yepes J, Dorrel RG, Vieira FRJ, Mach J, Morrissey J, Leon S, Lam F, Pelletier E, Camadro JM, Bowler C, Lesuisse E (2018) Endocytosis-mediated siderophore uptake as a strategy for Fe acquisition in diatoms. Sci Adv 4:1–14

Killian O, Kroth PG (2004) Presequence acquisition during secondary endocytobiosis and the possible role of introns. J Mol Evol. 58:712–721

Kong L, Price NM (2019) Functional CTR-type Cu(I) transporters in an oceanic diatom. Environ Microbiol 21:98–110

Kong L, Price NM (2020) Identification of copper-regulated proteins in an oceanic diatom, *Thalassiosira oceanica* 1005. Metallomics 12:1106–1117

Kropat J, Tottey S, Birkenbihl RP, Depège N, Huijser P, Merchant S (2005) A regulator of nutritional copper signaling in *Chlamydomonas* is an SBP domain protein that recognizes the GTAC core of copper response element. Proc Natl Acad Sci USA 102(51):18730–18735

Levy JL, Angel BM, Stauber JL, Poon WL, Simpson SL, Cheng SH, Jolley DF (2008) Uptake and internalisation of copper by three marine microalgae: Comparison of copper–sensitive and copper–tolerant species. Aquat Toxicol 89:82–93

Lommer M, Specht M, Roy AS, Kraemer L, Andreson R, Gutowska MA, Wolf J, Bergner SV, Schilhabel MB, Klostermeier UC, Beiko RG, Rosenstiel P, Hippler M, La Roche J (2012) Genome and low-iron response of an oceanic diatom adapted to chronic iron limitation. Genome Biol 13:R66, 1–20

Lowry OH, Rosebrough NJ, Farr AL, Randall RJ (1951) Protein measurement with the Folin Phenol Reagent. J Biol Chem 193:265–275

Maldonado MT, Allen AE, Chong JS, Lin K, Leus D, Karpenko N, Harris SL (2006) Copper dependent iron uptake in coastal and oceanic diatoms. Limnol Oceanogr 51:1729–1743

Marchetti A, Schruth DM, Durkin CA, Parker MS, Kodner RB, Berthiaume CT, Morales R, Allen AE, Armbrust EV (2012) Comparative metatranscriptomics identifies molecular bases for the physiological responses of phytoplankton to varying iron availability. Proc Natl Acad Sci USA. 109:E317–25

Martin-Jézéquel V, Tesson B. *Phaeodactylum tricornutum* polymorphism: an overview *In*: Advances in Algal Cell Biology (Heimann K. and Katsaros C., eds.) chapter 3, pp. 43–80. De Gruyter publishing group, 2013.

McLachlan J (1964) Some considerations of the growth of marine algae in artificial media. Can J Microbiol 10(8104):769–782

Merchant S, Bogorad L (1986) Regulation by copper of the expression of plastocyanin and cytochrome c_{552} in *Chlamydomonas reinhardi*. Mol Cell Biol 6(2):462–469

Moore JK, Braucher O (2008) Sedimentary and mineral dust sources of dissolved iron to the world ocean. Biogeosciences 5:631–656

Morrissey J, Bowler C (2012) Iron utilization in marine cyanobacteria and eukaryotic algae. Front Microbiol 3(43):1–13

Msilini N, Zaghdoudi M, Govindachary S, Lachaâl M, Ouerghi Z, Carpentier R (2011) Inhibition of photosynthetic oxygen evolution and electron transfer from the quinone acceptor Q_A^- to Q_B by iron deficiency. Photosynth Res 107(3):247–256

Murata N, Takahashi S, Nishiyama Y, Allakhverdiev SI (2007) Photoinhibition of photosystem II under environmental stress. Biochim Biophys Acta 1767:414–421

Nosenko T, Lidie KL, Van Dolah FM, Lindquist E, Cheng JF, Bhattacharya D (2006) Chimeric plastid proteome in the florida "red tide" dinoflagellate *Karenia brevis*. Mol Biol Evol 23:2026–2038

Nouet C, Motte P, Hanikenne M (2011) Chloroplastic and mitochondrial metal homeostasis. Trends Plant Sci 16:395–404

Peers G, Price NM (2006) Copper-containing plastocyanin used for electron transport by an oceanic diatom. Nature 441:341–344

Pierella Karlusich JJ, Lodeyro AF, Carrillo N (2014) The long goodbye: the rise and fall of flavodoxin during plant evolution. J Exp Bot 65:5161–5178

Pushnik JC, Miller GW (1989) Iron regulation of chloroplast photosynthetic function: Mediation of PS I development. J Plant Nutr 12(4):407–421

Rizkallah MR, Frickenhaus S, Trimborn S, Harms L, Moustafa A, Benes V, Gäbler-Schwarz S, Beszteri S (2020) Deciphering patterns of adaptation and acclimation in the transcriptome of *Phaeocystis antarctica* to changing iron conditions. J Phycol 56(3):747–760

Rogl H, Kosemund K, Kühlbrandt W, Collinson I (1998) Refolding of *Escherichia coli* produced membrane protein inclusion bodies immobilised by nickel chelating chromatography. FEBS Lett 432:21–26

Roncel M, González-Rodríguez AA, Naranjo B, Bernal-Bayard P, Lindahl AM, Hervás M, Navarro JA, Ortega JM (2016) Iron deficiency induces a partial inhibition of the photosynthetic electron transport and a high sensitivity to light in the diatom *Phaeodactylum tricornutum*. Front Plant Sci 7(1050):1–14

Roncel M, Yruela I, Kirilovsky D, Guerrero F, Alfonso M, Picorel R, Ortega JM (2007) Changes in photosynthetic electron transfer and state transitions in an herbicide-resistant D1 mutant from soybean cell cultures. Biochim Biophys Acta 1767(6):694–702

Rutherford AW, Renger G, Koike H, Inoue Y (1984) Thermoluminescence as a probe of Photosystem II. The redox and protonation states of the secondary acceptor quinone and O_2-evolving enzyme. Biochim Biophys Acta 767:548–556

Sambrook J, Russell DW (1989) Molecular Cloning: A Laboratory Manual. Cold Spring Harbor Laboratory Press, Cold Spring Harbor, New York

Sancho J (2006) Flavodoxins: sequence, folding, binding, function and beyond. Cell Mol Life Sci 63:855–864

Sandmann G (1986) Formation of plastocyanin and cytochrome c_{553} in differents species of blue-green algae. Arch Microbiol 145:76–79

Schindelin J, Arganda-Carreras I, Frise E, Kaynig V, Longair M, Pietzsch T, Preibisch S, Rueden C, Saalfeld S, Schmid B, Tinevez J-Y, White DJ, Hartenstein V, Eliceiri K, Tomancak P, Cardona A

(2012) Fiji: An open-source platform for biological-image analysis. Nat Methods 9(7):676–682

Sétif P. Electron transfer from the bound iron–sulfur clusters to ferredoxin/flavodoxin: kinetic and structural properties of ferredoxin/flavodoxin reduction by photosystem I. In: (Golbeck JH, ed.) Photosystem I: the Ligth Driven Plastocyanin:Ferredoxin Oxidoreductase. Advances in Photosynthesis and Respiration 24, pp. 439-454. Springer, Dordrecht, The Netherlands 2006

Strickland JDH, Parsons TR (1972) A practical handbook of seawater analysis. Bulletin Fisheries Research Board of Canada 167:1–311

Strzepek RF, Harrison PJ. (2004) Photosynthetic architecture differs in coastal and oceanic diatoms. Nature 431:689–692

Szabo E, Colman B (2007) Isolation and characterization of carbonic anhydrases from the marine diatom *Phaeodactylum tricornutum*. Physiol Plant 129(3):484–492

Twining BS, B. Baines SB (2013) The trace metal composition of marine phytoplankton. Annu Rev Mar Sci 5:191–215

Ubbink M, Ejdebäck M, Karlsson BG, Bendall DS (1998) The structure of the complex of plastocyanin and cytochrome *f*, determined by paramagnetic NMR and restrained rigid-body molecular dynamics. Structure 6:323–335

Vavilin DV, Ducruet J-M (1998) The origin of 115–130 °C thermoluminescence bands in chlorophyll-containing material. Photochem Photobiol 68(2):191–198

Vavilin DV, Matorin DN, Rubin AB (2002) High-temperature thermoluminescence of chlorophyll as a method to study lipid peroxidation in planktonic algae. Arch Hydrobiol 153(4):685–701

Yamada, S., Park, S.Y., Shimizu, H., Koshizuka, Y., Kadokura, K., Satoh, T., Suruga, K., Ogawa, M., Isogai, Y., Nishio, T., Shiro, Y., and Oku, T. (2000) Structure of cytochrome c_6 from the red alga *Porphyra yezoensis* at 1.57 Å resolution. Acta Crystallogr. D. Biol. Crystallogr. 56:1577–1582

Table 1. General physiological and biochemical parameters of *P. tricornutum* transformed cells and cultures under iron-deficient conditions, expressed as the percentage of that of WT cells.

Parameter (after 15 days of growth)[a)]	**WT**	**#30**	**#45**	**#79**
Cells per mL	100%	140%	159%	163%
Specific growth rate (μ)	100%	113%	118%	119%
Total Chl per mL	100%	144%	194%	194%
Chl *a* per mL	100%	150%	206%	212%
Chl *c* per mL	100%	150%	216%	211%
Total carotenoids per mL	100%	172%	236%	213%
Total Chl per cell	100%	120%	140%	137%
Total carotenoids per cell	100%	125%	150%	135%
Cell circularity	100%	130%	133%	115%
Cell volume	100%	90%	139%	132%
Cell surface	100%	84%	110%	112%
Net photosynthetic rate per cell	100%	122%	213%	235%

[a)]See the Materials and Methods section for more details.

Table 2. Maximum quantum yield of PSII (F_v/F_m), photosynthetically active radiation intensity (PAR) for relative maximum electron transport rate ($rETR_{max}$), relative electron transport rate (rETR) at maxima photosynthetically active radiation intensity (PAR_{max}), maximal P_{700}^+ signal upon full oxidation (P_m) and half-life time ($t_{1/2}$) of the P_{700}^+ re-reduction in iron-replete (+Fe) WT and iron-deficient (–Fe) WT cells and the #30, #45 and #79 mutants.

Parameter	**WT+Fe**	**WT–Fe**	**#30–Fe**	**#45–Fe**	**#79–Fe**
F_v/F_m	0.632±0.004	0.331±0.014	0.381±0.055	0.384±0.036	0.425±0.044
PAR for ETR_{max} (µmol m^{-2} s^{-1})[a)]	500	150	200	350	350
rETR (at PAR_{max})[b)]	22.55	0.08	1.48	3.57	4.63
P_m	0.683±0.043 (--)	0.093±0.011 (100%)[c)]	0.110±0.008 (118%)[c)]	0.105±0.003 (113%)[c)]	0.112±0.007 (120%)[c)]
$t_{1/2}$ (ms)	4.45±0.23	11.82±0.93	5.35±0.35	6.06±0.37	5.84±0.35

[a)]Light intensity for $rETR_{max}$; [b)]rETR values at 1957 µmol m^{-2} s^{-1} light intensity; [c)]values as percentage of that of WT–Fe cells.

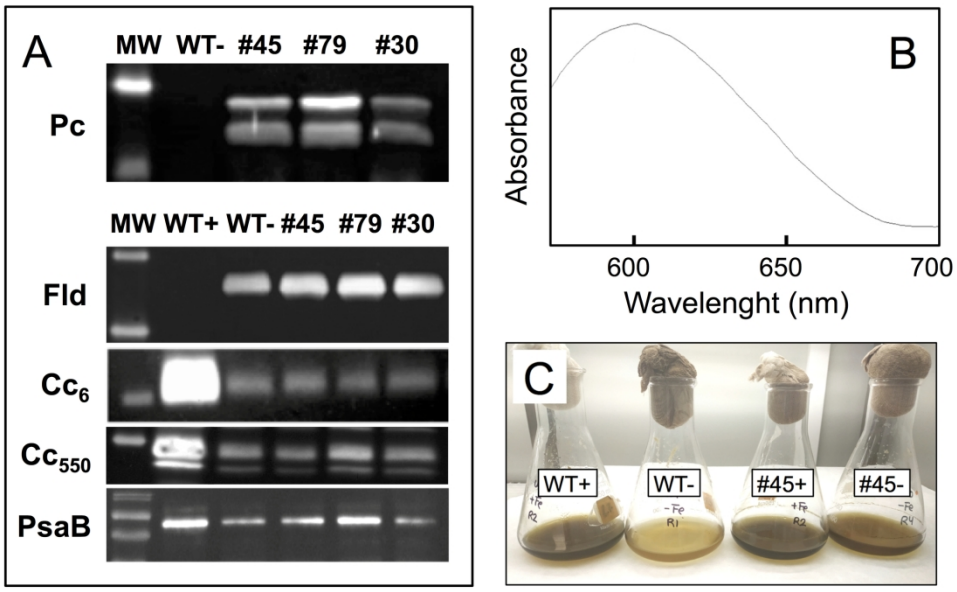

Figure 1

Figure 1

189x128mm (300 x 300 DPI)

Figure 2

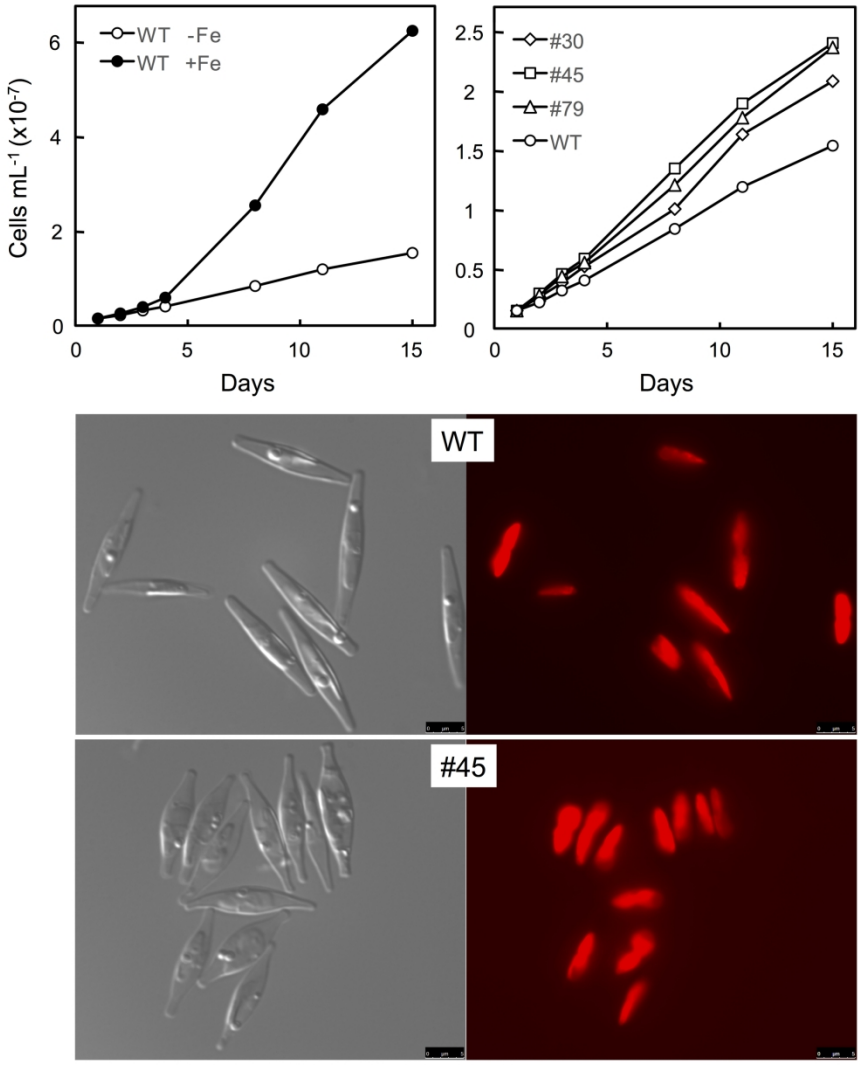

Figure 2

188x247mm (300 x 300 DPI)

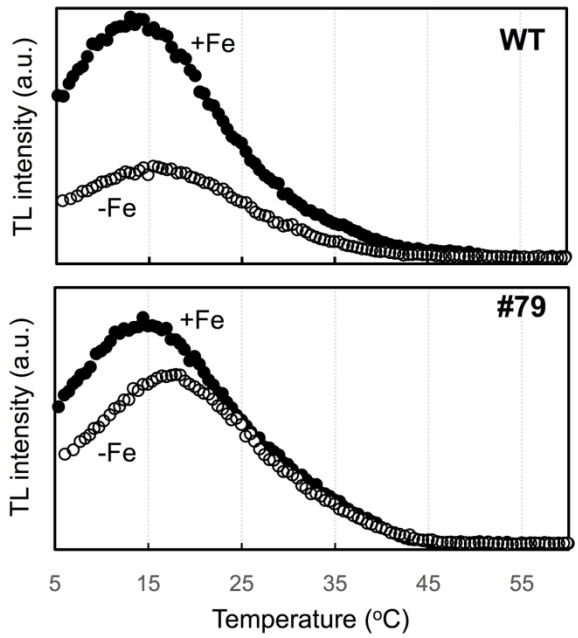

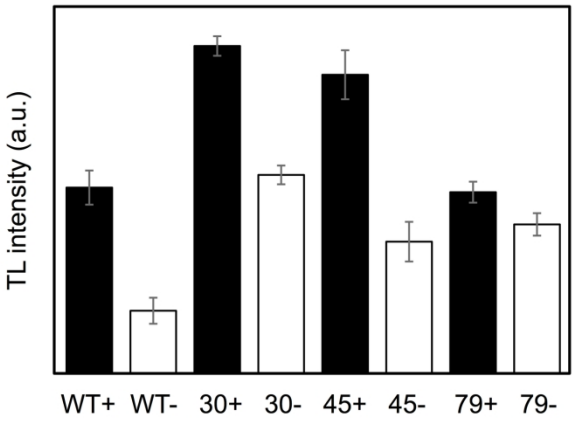

Figure 3

Figure 3

120x229mm (300 x 300 DPI)

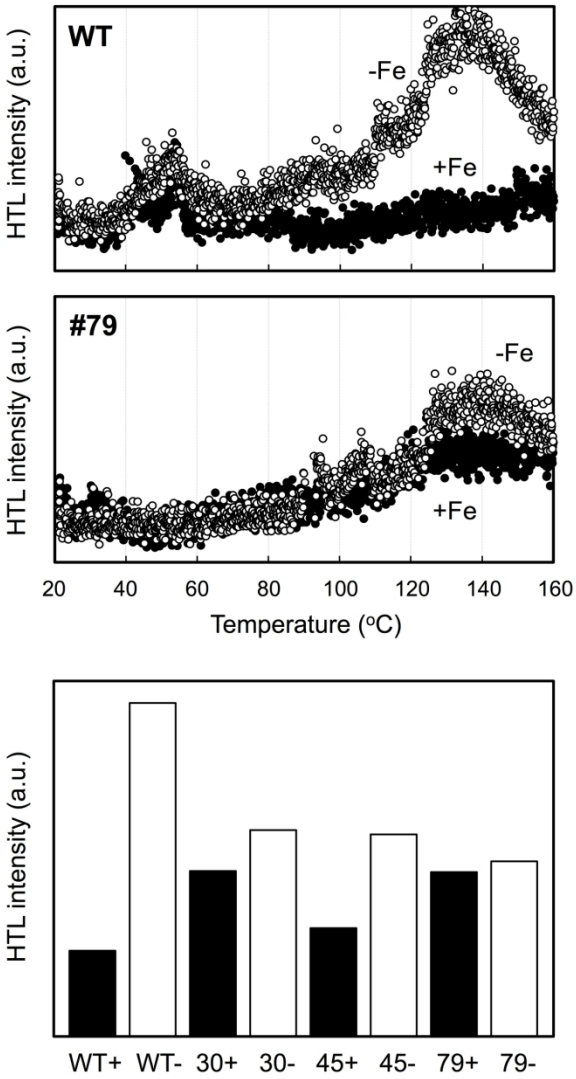

Figure 4

Figure 4

129x236mm (300 x 300 DPI)

Figure 5

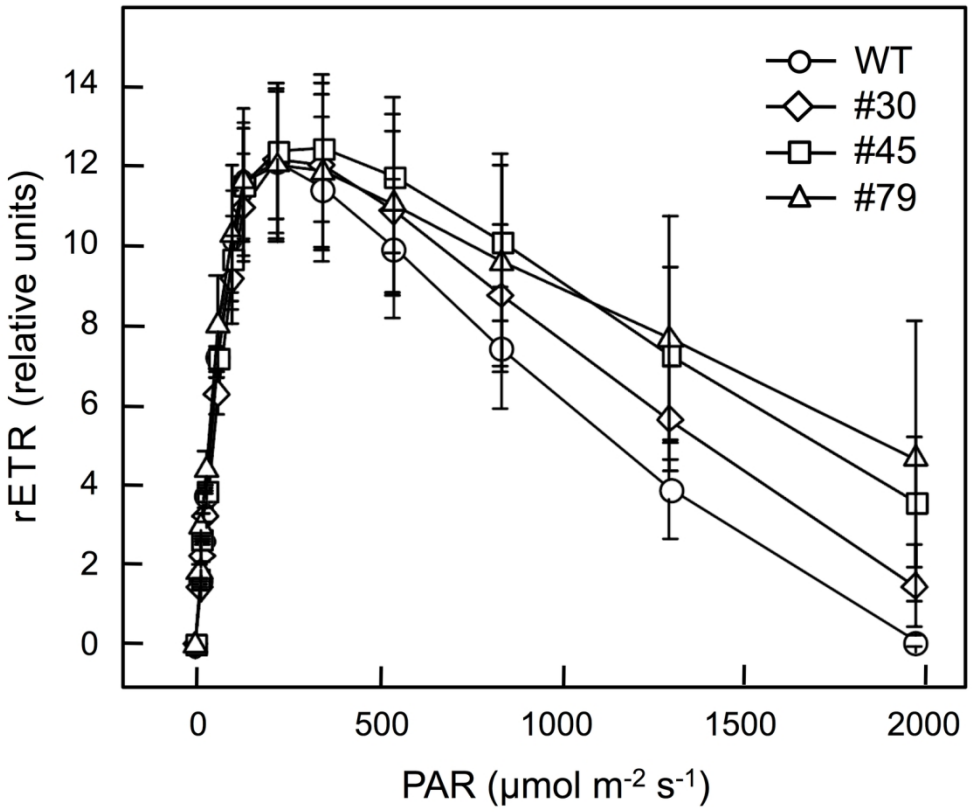

Figure 5

149x138mm (300 x 300 DPI)

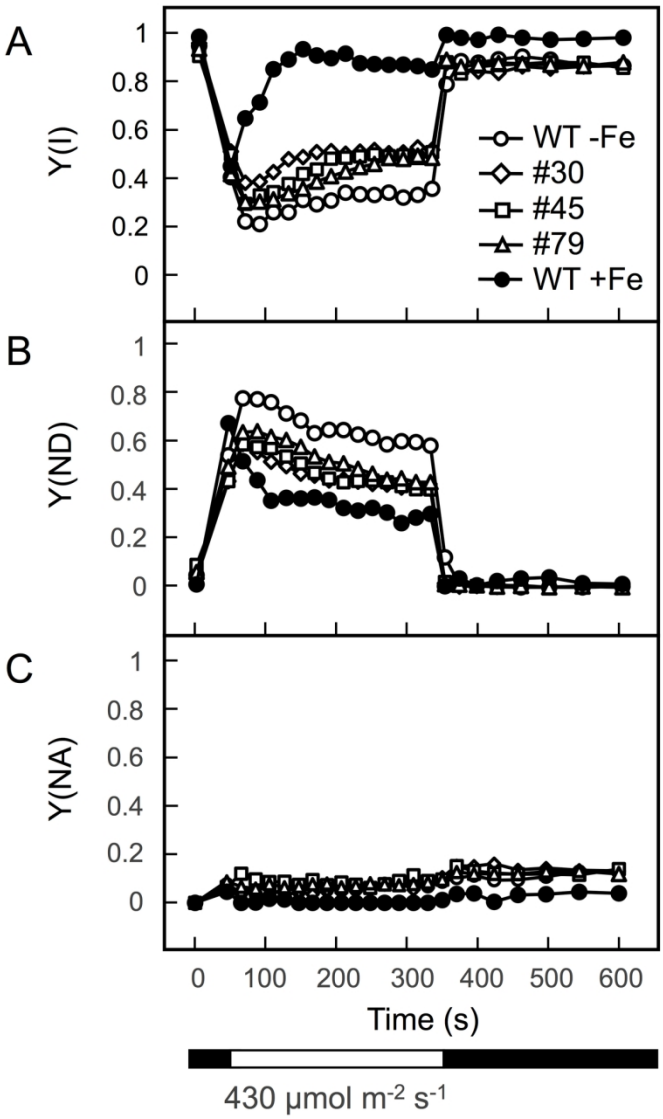

Figure 6

Figure 6

114x190mm (300 x 300 DPI)